Synthesis of Nanorods with Ni Cores and Porous Silica Coatings

**N. Shukla · J. B. Miller · E. Coletta ·
A. D. Ondeck · V. Pushkarev · A. J. Gellman**

Abstract Nanorods with a Ni core and a silica coating have been prepared using a one-step synthesis and characterized using a variety of methods. Nitrogen adsorption isotherms have been used to characterize the pore size and the internal surface area of the silica shells grown on the Ni nanorods. Spectroscopic characterization of CO adsorbed on the Ni nanoparticle cores has been used to verify that the pore structure of the silica shells allows CO to access the Ni core; this property is critical to the use of core–shell structures as industrial catalysts. To demonstrate their resistance to physical and chemical degradation, the properties of the silica-coated Ni nanoparticles have been measured both before and after treatment at high temperature (623 - 1073 K) and exposure to a reducing atmosphere (hydrogen gas). Annealing at high temperatures reduces, but does not eliminate, the porosity of the silica shells.

Keywords Nanoparticulate catalyst · Silica coatings · Ni nanoparticles

N. Shukla · J. B. Miller · A. J. Gellman
US DOE—National Energy and Technology Laboratory,
626 Cochrans Mill Rd., Pittsburgh, PA 15236-0940, USA

N. Shukla (✉)
Institute for Complex Engineered Systems, Carnegie Mellon
University, 5000 Forbes Ave., Pittsburgh, PA, USA
e-mail: nisha@andrew.cmu.edu

J. B. Miller · E. Coletta · A. D. Ondeck · V. Pushkarev ·
A. J. Gellman
Department of Chemical Engineering, Carnegie Mellon
University, 5000 Forbes Ave., Pittsburgh, PA 15213, USA

1 Introduction

Over the past decade there has been widespread interest in wet chemical synthesis of nanoparticles and their applications in various fields. One area in which nanoparticles can play an important role is heterogeneous catalysis. There have been many reports of nanoparticle synthesis for applications in catalysis, but two major challenges must be addressed before such synthetically produced nanoparticulate catalysts can be used commercially to their full potential [1–3]. The first is the development of simple, cost-effective synthetic routes that yield nanoparticles with uniform shape and size and expose a uniform set of crystal planes selected to provide high catalytic activity and selectivity. The second challenge is the development of strategies to make the particles resistant to sintering in the extreme chemical and thermal environments that characterize many important catalytic processes. Sintering destroys the shapes of the nanoparticles and causes changes in particle size distribution, typically increasing the mean particle size. Sintering and adsorbate induced changes in particle shape undermine some of the potential advantages that chemically synthesized nanoparticulate catalysts have over conventional particulate metal catalysts. There are many strategies to avoid the sintering of nanoparticulate catalysts; the method explored in this work has been to coat the nanoparticles with protective silica coatings of controlled thicknesses. It is challenging to control the thickness of the silica coating; however, it is equally important that the silica coating be porous so that reactant molecules have access to the nanoparticle core during catalysis. Such silica shells can provide contaminant resistance [4–6], while also serving to reduce sintering and thus, improved thermal stability [7–12]. The pores of the silica shells can be tailored in size and chemical properties such that reactant

species can penetrate the shell to reach the surface of the metallic nanoparticles, while contaminant molecules cannot. Similarly, the silica shells can retard the diffusion of metal atoms from the core to the exterior of the particle shell where they can sinter into large metallic clusters [26]. The objective of silica coating methods is to obtain maximum thermal stability with minimal loss of reactivity.

Silica coatings on nanoparticles can be synthesized by a variety of methods [13–17] including sol–gel chemistry [18] and the use of microemulsions [19]. Each method can be controlled to produce different coating thicknesses with different porosities and pore sizes. The shapes of the silica coatings are also dependent on the synthesis parameters and may conform to the shape of the core particles or be spherical [20, 21].

In addition to providing control of critical nanoparticle properties, synthetic methods must be simple and scalable if they are to be considered for practical applications. Most methods for creating core–shell nanoparticles use a two-step synthesis process that prepares the metal cores in one step and the silica shells or a second metal shell in a second step [20–22]. Our work demonstrates a one-step synthesis of silica shells on Ni nanoparticle cores. The method also allows production of spherical and shape-controlled shells. Although significant effort has gone into the synthesis and morphological characterization of shape-controlled Ni nanoparticles [23–25] with porous silica coatings, our primary aim has been to evaluate the porosity of the silica coating using N_2 adsorption and FTIR measurements of CO adsorption. This has allowed a correlation between porosity measurements and CO adsorption. Finally, high-temperature thermal treatments, in both air and hydrogen atmospheres, have been used to show that the silica coated nanoparticles are more resistant to sintering than a commercial silica-supported Ni catalyst treated in the same manner.

2 Experimental

Silica coated Ni nanoparticles were synthesized using a one-step synthesis process. In a typical synthesis, the liquid surfactant Brij 56 (polyethylene glycol hexadecyl ether, average $M_n = 683$) was dissolved in 100 ml of cyclohexene to a concentration of 0.012 M and stirred for 30 min at ~333 K in a three neck glass flask. A 0.001 M solution of Ni(II) nitrate hexahydrate or nickel chloride dissolved in 5 mL of distilled water was added to the colorless solution of surfactant and solvent. At this stage the color of the solution turns to light green. Heating of the mixture continued for another 10 min. Next, 3 mL of hydrazine hydrate solution (reagent grade, 50–60%) or sodium borohydride was added to the solution of surfactant and Ni precursor at 333 K. The solution immediately turned from light green to light blue to light purple and pink until all the hydrazine solution had been added. Next, 25 mL of ammonium hydroxide solution (33%) was added to the reaction mixture. Finally, 30 mL of TEOS was added very slowly (dropwise). The reaction mixture was heated and allowed to stir for 3 h. After the synthesis, the Ni nanoparticles were centrifuged and washed with polar solvent to remove the excess surfactant [12–17].

The synthesis parameters were modified to change the shape and the size of the silica coated Ni nanoparticles. To change the shape and the size of both the Ni core and the silica shell, the amounts of the ammonium hydroxide and TEOS solutions and the reaction time were varied.

2.1 X-ray Diffraction and X-ray Florescence

X-ray diffraction patterns were obtained from a Panalytical X'Pert Pro X-ray diffractometer. A Cu radiation source was used with a polycapillary lens and a Ni filter to provide the incident beam. Samples for XRD were prepared by evaporating solvent from a colloidal Ni nanoparticle solution followed by drying in a vacuum oven to form powder. XRD analyses of silica coated Ni nanoparticles did not indicate long range ordering within the samples; this observation probably reflects the small size of the Ni nanoparticles and their thin silica coatings. X-ray fluorescence (XRF) measurements were performed on a Panalytical MiniPal 4 XRF spectrometer. Loose powder samples were placed in a plastic cup with a bottom X-Ray window made of polyvinylidene chloride (Saran Wrap). A rhodium target X-ray source was used with 15 kV and 0.28 mA power settings. Scans were run for 30 s in air with no filter. The XRF measurement of the silica coated sample confirmed the presence of both silica and Ni.

2.2 Transmission Electron Microscopy (TEM)

TEM studies were conducted using a JEOL JEM-2000 EX II microscope operating at 200 keV with a Gatan Camera. The high resolution TEM studies were done using a Technai F20 FEG/HRTEM/STEM with a Gatan imaging filter and an energy dispersive X-ray spectroscopy system. TEM samples were prepared by evaporation of 20 μl of the colloidal Ni nanoparticle solution in propanol onto a carbon-coated, 200 mesh, Cu TEM grid. To induce sintering, Ni nanoparticles were deposited onto a carbon-coated TEM grid and annealed in air at 650 K for 15 min.

2.3 Characterization of Shell Porosity by N_2 Desorption

The pore size distribution and surface area of the nanoparticles were measured by N_2 desorption methods using a

Quantachrome Nova 2200e instrument. Surface areas were calculated from the desorption isotherm using the BET method. The samples for BET measurements were prepared by centrifuging the colloidal solution of Ni nanoparticles, drying overnight at 373 K in a vacuum oven, and finally drying in air at 623 K for 1 h in a conventional oven.

2.4 FTIR Measurements for CO Adsorption

CO adsorption on powdered silica-coated Ni nanoparticles was studied using diffuse reflectance infrared spectroscopy (DRIFT). All measurements were conducted in a Nicolet 6700 FTIR spectrometer equipped with a liquid N_2 cooled HgCdTe detector and a Spectra-tech horizontal diffuse reflection spectroscopic accessory. The IR cell used for these measurements was a compact, vacuum tight Pyrex glass tube with ZnSe windows. For all measurements, 50 µg of dried silica coated nanoparticles were first mixed with 150 µg of CaF_2 (ACS purity) and dried at 573 K for 15 min in the IR cell. The IR cell was then evacuated and filled with 760 Torr of H_2 and the mixture was reduced at 573 K for 15 min as a pretreatment. Finally, the cell was evacuated, cooled to room temperature and filled with 5 psi of CO for a few minutes. The IR spectra were acquired as 256 scans in the region 1000–4000 cm^{-1} with a spectral resolution of 4 cm^{-1}.

2.5 Temperature Programmed Reduction (TPR) Measurements

Temperature Programmed Reduction (TPR) experiments were preformed using an Altamira 200-R-HP instrument, equipped with a thermal conductivity (TC) detector. Approximately 0.03 g of a granular sample, which had been dried ex-situ in air at 623 K, was loaded into a glass-lined, stainless steel reactor tube and held in place by quartz wool plugs. The sample was first heated to 423 K in flowing Ar to desorb residual moisture, and was then cooled to 313 K. The treatment gas was changed to 4% H_2 in Ar, and the sample was heated to 923 K at a rate of 10 K/min. The TC detector reported a signal proportional to the difference between the thermal conductivities of the inlet and outlet streams as a measure of hydrogen consumed during reduction of the sample.

Ni(II) nitrate hexahydrate (>99.99%), Ni (II) chloride, Brij 56, hydrazine hydrate, ammonium hydroxide solution (30% solution), propanol, tetraethyl orthosilicate (TEOS, 99%), and cylcohexene were purchased from Sigma-Aldrich and were used without purification. A Ni/SiO_2–Al_2O_3 catalyst (66 wt% Ni) was obtained from Alfa Aesar for use as a reference in the TPR experiments.

3 Results

TEM imaging has been used to show that our one pot synthesis method produces nanorods with Ni cores and silica shells. Figures 1 and 2 shows the bright field TEM images of silica-coated Ni nanoparticles as deposited and after annealing at 650 K for 15 min in air. The images in Fig. 1a show that our synthesis allows the silica coatings to conform to the shape and size of the Ni cores. Although not shown in this paper, our synthesis method can, under other growth conditions, deliver silica coatings that are spherical and independent of the shape of the Ni core. Typically, spherical silica coatings are formed at shorter reaction times. An important feature of our synthesis is that the Ni cores grow in long rods (Fig. 1a) which are 100–900 nm in length. The Ni cores are formed of spherical Ni nanoparticles packed into a nanorod. It appears from Fig. 1a that the Ni nanoparticles pack randomly to form rods surrounding by a thin ($\sim$15 nm) silica shell. HRTEM shows (Fig. 1b–e) that the Ni nanoparticles are spherical ($\sim$5 nm in diameter) and pack within the silica shell. Annealing of the silica-coated Ni nanoparticles in a flow of air at 650 K in a rapid thermal processor does not induce sintering of the rods in the sense that there is no evidence of transport of Ni through the shell and agglomeration of Ni outside the shells (Fig. 2a, b). Resistance to sintering is important for application of Ni nanoparticles as catalysts.

In order for the Ni nanoparticles with silica shell to be catalytically active, the silica shell must be sufficiently porous to allow reactants to have access to the surface of Ni nanoparticles and to allow products to depart. Figure 3 shows the pore size distribution and surface area measurements of silica-coated Ni nanoparticles determined by N_2 desorption after annealing at various temperatures in the air for 1 h. At all annealing temperatures, the pore size distributions display a sharp maximum at $\sim$3.8 nm; this is the characteristic diameter of the pores in the silica shells [26]. As the material was heated to higher temperatures, shell sintering resulted in reduced porosity—a reduction in the pore volume at 3.8 nm. Sintering also causes a corresponding loss of silica surface area, from 109 m^2/g at 623 K to 100 m^2/g at 773 K, and finally to 78 m^2/g at 873 K. Loss of porosity upon heat treatment of silica coatings has been reported in several studies [22, 23].

Spectroscopic characterization of the adsorption of CO on the metallic cores of the nanoparticles has been used to probe the porosity of the silica shells. Figure 4 shows the FTIR spectra of CO adsorbed onto samples of SiO_2 coated Ni nanoparticles that have different Ni-core dimensions. Figure 4 shows a spectrum obtained following CO adsorption on Ni nanoparticle rods (>100 nm in length and diameter of 20 nm). The CO FTIR spectrum displays an
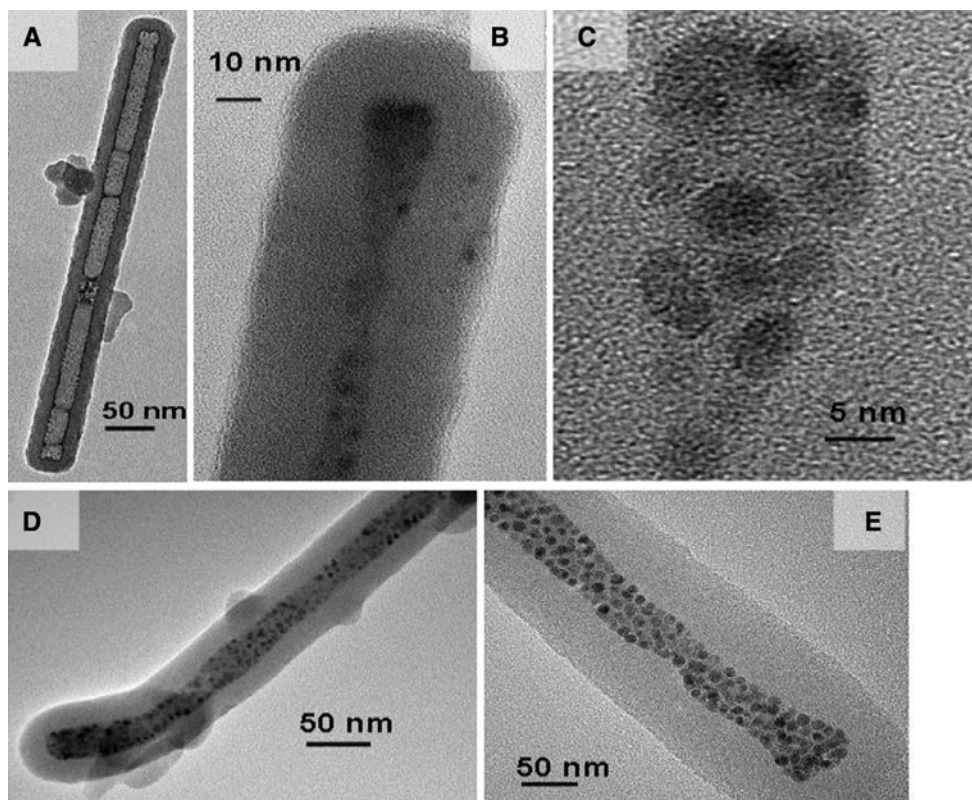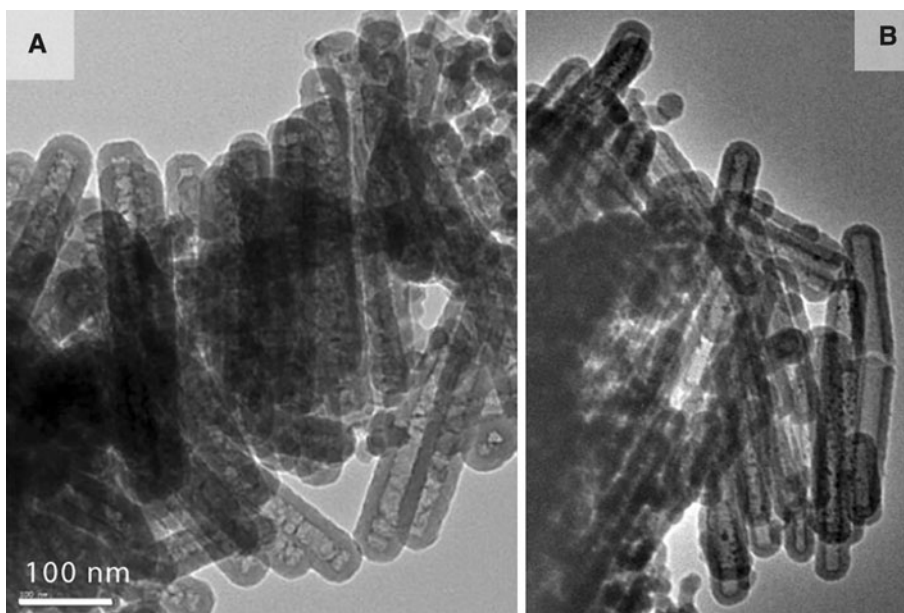
Fig. 1 Bright field TEM images of spherical Ni nanoparticles packed to form nanorods. The Ni rods are coated with silica shells that are 20–50 nm thick

Fig. 2 Bright field TEM image of silica coated Ni nanoparticles. **a** At 300 K. **b** After annealing at 650 K for 15 min in air. No sintering is observed following annealing

intense vibrational feature at ~ 2040 cm^{-1} which is characteristic of CO adsorbed on Ni [27–35]. The observation of vibrations associated with CO on Ni is a significant result because it confirms that CO, a key component of synthesis gas, can penetrate the protective silica core to access the metallic core.

Several studies [28–36] have reported an intense band at ~ 2050 cm^{-1} and a shoulder at ~ 2070 cm^{-1} for room temperature adsorption of CO on Ni surfaces or on Ni supported on silica. On Ni(100), CO exhibits stretching frequencies of 2050 and 1950 cm^{-1} for atop and bridging sites, respectively [31, 32]. Another study reported
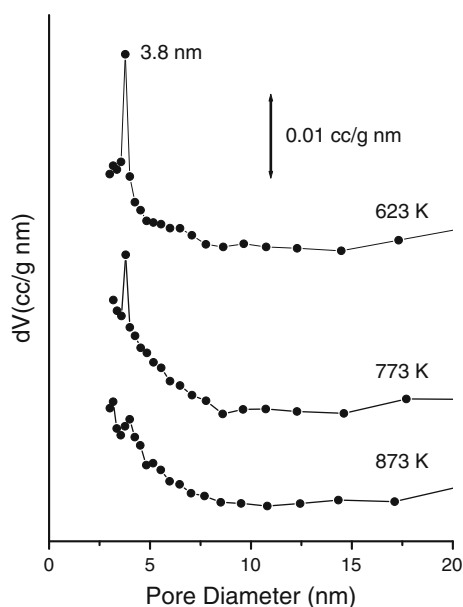
Fig. 3 Pore size distribution as measured by N_2 adsorption for Ni nanoparticles coated with silica and annealed at various temperatures. BET surface areas following annealing are 109 m^2/g (623 K), 100 m^2/g (773 K) and 78 m^2/g (873 K)

Fig. 4 FTIR spectra of CO adsorption on silica-coated Ni nanoparticles annealed to 573 K for 1 h

vibrational bands at 2198 cm^{-1} (CO adsorbed on Ni^{2+}), 2046 cm^{-1} (CO linearly adsorbed), 1885 cm^{-1} (CO bridged) and 1797 cm^{-1} (three-fold coordinated) for CO adsorbed on Ni supported on silica [33]. In contrast with these reports, we observe only a very strong band at 2040 cm^{-1}. This difference may reflect the fact that our Ni particles are in more intimate contact with the silica than Ni nanoparticles supported on the surfaces of silica supports.

Additional FTIR experiments were performed to further confirm that the CO adsorption occurred on the Ni surface and that the silica coatings are porous. The results of these experiments are shown in Fig. 5. We characterized adsorption of CO on pure silica to verify that the vibrational peak shown in Fig. 4 is due only to CO adsorption on the Ni nanoparticle cores and not due to interaction or adsorption of CO on silica. No vibrational peaks were observed in the region 2040–2060 cm^{-1} for the silica sample suggesting that CO does not adsorb on pure silica (Fig. 5a). In the next experiment, CO adsorption was characterized on silica coated Ni nanoparticles that had been annealed to 1073 K for 1 h. We know that the silica shell porosity decreases with annealing at higher temperatures. Therefore, we expect that there should be less CO adsorbed on the Ni nanoparticle and that the CO absorption peak should be much weaker than on the sample annealed at only 573 K (Fig. 4). As observed in Fig. 5b, a weak vibrational peak is observed at 2050 cm^{-1} suggesting that there is limited adsorption of CO on Ni nanoparticles and
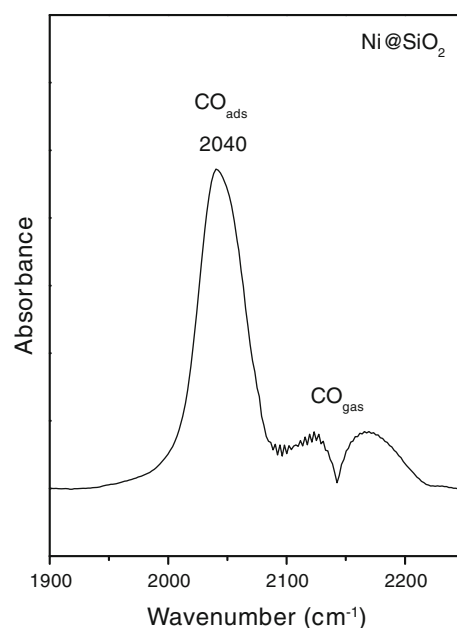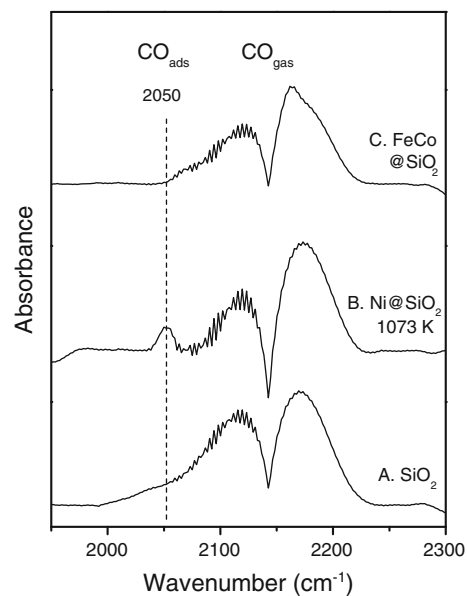

Fig. 5 FTIR spectra of CO adsorption on **a** silica, **b** silica-coated Ni nanoparticles annealed to 1073 K, and **c** FeCo nanoparticles coated with thick non-porous silica shells

that the transport of gases through the silica coatings is hindered following annealing at high temperatures. In addition, we examined a sample of silica coated FeCo made by a different synthesis method. The synthesis of silica coated FeCo is similar to that of silica coated Ni except that the amount of surfactant (Brij56) was four times higher. Higher amount of Brij56 in our synthesis produces thicker silica shells. BET measurements show
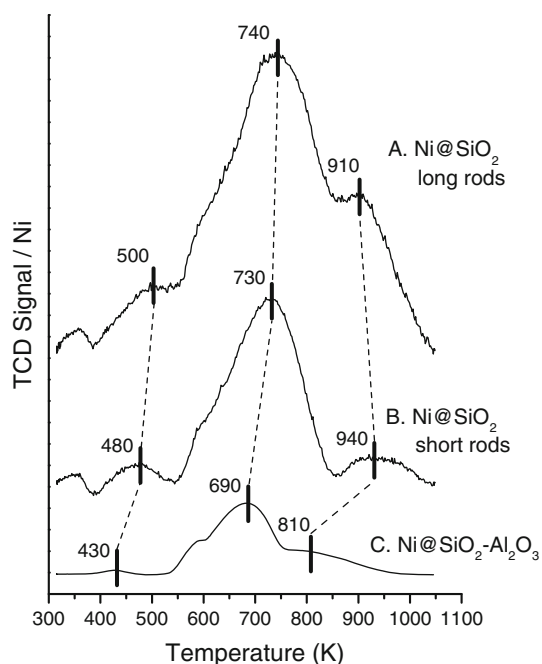
Fig. 6 Temperature programmed reduction of two samples of silica-coated Ni nanoparticles and a commercially available Ni/SiO$_2$-Al$_2$O$_3$. All samples were annealed in air at 623 K before TPR analysis. Major reduction features appear at significantly higher temperatures in the silica coated Ni nanoparticles samples than in the commercial Ni on silica-alumina sample

that these silica coated FeCo nanoparticles have non-porous shells. Furthermore, as shown in Fig. 5c, the FeCo nanoparticles coated with non-porous silica did not display any vibrational peak in the region 2040–2050 cm^{-1} suggesting that there was no adsorption of CO. The data presented in Figs. 4 and 5 demonstrates that CO can penetrate the porous silica shells on the Ni nanoparticles to access the catalytic Ni core of the nanorods.

Once the porosity of the silica coatings of Ni nanoparticle was demonstrated, further experiments were performed to compare the silica coated Ni nanoparticles with a commercially available Ni catalyst supported on silica-alumina. Figure 6 shows the results of TPR measurements in hydrogen of two silica-coated Ni nanoparticle samples (Figs. 6a, b) and the Ni supported on silica alumina (Fig. 6c). The sample in Fig. 6b has longer nanorods (>100 nm in length) than the one in Fig. 6a (<100 nm in length). All materials were annealed in air at 673 K before TPR analysis. Reduction profiles for both silica coated Ni nanoparticle samples display features that correspond to those observed for the commercial catalyst. Reduction features that appear at temperatures below 573 K have been attributed to the conversion of Ni^{3+} (Ni$_2$O$_3$) to Ni^{2+} (NiO) [37–44]. NiO which interacts only very weakly with the oxide support/host [36–39], reduces at temperatures between 573 and 773 K; this is the dominant species in all

three samples. Temperatures above 773 K are required to reduce NiO species that are stabilized by intimate interaction with the oxide support/host [40, 42, 44]. The main nanoparticle reduction features appear at significantly higher temperatures than those for the commercial supported Ni catalyst. The difference is largest for the high temperature reduction feature which occurs at ∼100 K higher in the nanoparticulate samples than in the commercial supported Ni. These results are consistent with stabilization of the nanoparticulate NiO cores through interaction with their silica shells at the large interface between them.

Significant differences among the total amount of hydrogen consumed by the samples (the area under the TPR curves) are also observed. When normalized to their Ni contents, the nanoparticulate samples consume more than twice as much hydrogen as the commercial catalyst (the profile for the commercial sample has been magnified by a factor of two for display in Fig. 6c). This observation likely reflects higher Ni surface area in the nanoparticulate catalyst and thus, the greater relative amount of oxygen uptake during oxidation prior to the TPR measurements.

4 Conclusions

We have developed a one step, wet chemical synthesis for preparation of nanorods with Ni cores encased in thin silica coatings. Characterization of the nanoparticles by N$_2$ adsorption shows that the coatings are porous and that they retain porosity even when calcined to temperatures as high as 873 K. As demonstrated by IR spectroscopy, the shell pores allow CO access to the Ni cores of the nanoparticles; this property is critical for applications in catalysis. Reduction studies of the nanoparticles suggest that Ni in the nanoparticles is more highly dispersed and has stronger interactions with the silica shell than does Ni in traditional supported catalysts. Our results illustrate the potential of porous oxide coatings to protect nanoparticulate catalysts in extreme environments.

References

1. Rioux RM, Song H, Grass M, Habas S, Niesz K, Hoefelmeyer JD, Yang P, Somorjai GA (2006) Top Catal 39:167
2. Kweskin SJ, Rioux RM, Habas SE, Komvopoulos K, Yang P, Somorjai GA (2006) J Phys Chem B 110:15920
3. Bratlie KM, Lee H, Komvopoulos K, Yang P, Somorjai GA (2007) Nanoletters 7:3097

4. Gerion D, Pinaud F, Williams SC, Parak WJ, Zanchet D, Weiss S, Alivisatos AP (2001) J Phys Chem B 105:8861
5. Le Y, Hou P, Wang J, Chen JF (2010) Mater Chem Phys 120:351
6. He Rong, You X, Shao J, Gao F, Pan B, Cui D (2007) Nanotechnology 18:315601
7. Lee DC, Mikulec FV, Pelaez JM, Koo B, Korgel BA (2006) J Phys Chem B 110:11160
8. Philipse AP, Bruggen MPBV, Pathmamanoharan C (1994) Langmuir 10:92
9. Aslam M, Fu L, Dravid V (2005) J Colloid Interface Sci 290:444
10. Yi DK, Selvan ST, Lee SS, Papaefthymiou GC, Kundaliya D, Ying JY (2005) J Am Chem Soc 127:4990
11. Park JN, Forman AJ, Tang W, Cheng J, Hu YS, Lin H, McFarland EW (2008) Small 10:1694
12. Arnal PM, Comotti M, Schuth F (2006) Angew Chem Int Ed 45:8224
13. Yu KMK, Thompsett D, Tsang SC (2003) Chem Commun 13:1522
14. Jana NR, Earhart C, Yang JY (2007) Chem Mater 19:5074
15. Tago T, Shibata Y, Hatsuta T, Miyajima K, Kishida M, Tashiro S, Wakabayashi K (2002) J Mater Sci 37:977
16. Tago T, Nagase R, Hatsuta T, Kishida M, Wakabayashi K (2000) J Jpn Soc Powder Powder Metall ICF8: 763
17. Takenaka S, Umebayashi H, Tanabe E, Matsune H, Kishida M (2007) J Catal 245:392
18. Kobayashi Y, Correa-Duarte MA, Liz-Marzan LM (2001) Langmuir 17:6375
19. Hyashi H, Chen LZ, Tago T, Kishida M, Wakabayashi K (2002) Appl Catal A 231:81
20. Obare SO, Jana NR, Murphy CJ (2001) Nano Lett 11:601
21. Botell P, Corma A, Navarro MT (2007) Chem Mater 19:1979
22. Grzelczak M, Rodriguez-Gonzalez B, Perez-Juste J, Liz-Marzan LM (2007) Adv Mater 19:2262
23. Carenco S, Boissiere C, Nicole L, Sanchez C, Floch PL, Mezailles N (2010) Chem Mater 22:1340
24. Chen DH, Wu SH (2000) Chem Mater 12:1354
25. Khanna PK, More PV, Jawalkar JP, Bharte BG (2009) Mater Lett 63:1384
26. Yao X, Zhang L, Wang S (1995) Sens Actuators B Chem 24–25:347
27. Sato S, Takahashi R, Sodesawa T, Tanaka R (2003) Bull Chem Soc Jpn 76:217
28. Mihaylov M, Hadjiivanov K, Knozinger H (2001) Catal Lett 76:59
29. Rao KM, Spoto G, Zecchina A (1989) Langmuir 5:319
30. Heiz U (1998) Appl Phys A 67:621
31. Lauterbach J, Wittmann M, Kuppers J (1992) Surf Sci 279:287
32. Coulter K, Xu X, Goodman DW (1994) J Phys Chem 98:1245
33. Ueckert T, Lamber R, Jaeger NI, Schubert U (1997) Appl Catl A 155:75
34. Storozhev PY, Arean CO, Garrone E, Ugliengo P, Ermoshin VA, Tsyganenko AA (2003) Chem Phys Lett 374:439
35. Rupprechter G, Dellwig T, Unterhalt H, Freund HJ (2001) Top Catal 15:19
36. Zhu X, Zhang YP, Liu CJ (2007) Catal Lett 118:306
37. Ermakova MA, Ermakov DY (2002) Catal Today 77:225
38. Takenaka S, Kobayashi S, Ogihara H, Otsuka K (2003) J Catal 217:79
39. Venugopal A, Naveen Kumar S, Ashok J, Hari Prasad D, Durga Kumari V, Prasad KBS, Subrahmanyam M (2007) Int J Hydrogen Energy 32:1782
40. Gao J, Hou Z, Guo J, Zhu Y, Zheng X (2008) Catal Today 131:278
41. Hadjiivanov K, Mihaylov M, Klissurski D, Stefanov P, Abadjieva N, Vassileva E, Mintchev L (1999) J Catal 185:314
42. He S, Jing Q, Yu W, Mo L, Lou H, Zheng X (2009) Catal Today 148:130
43. Li J, Lu G (2004) Appl Catal A Gen 273:163
44. Borowiecki T, Denis A, Gac W, Dziembaj R, Piwowarska Z, Drozdek M (2004) Appl Catal A Gen 274:259